Single-wavelength transmission at 1.1-Tbit/s net data rate over a multi-modal free-space optical link using commercial devices

ZHOUYI HU, YIMING LI*, DAVID M. BENTON, ABDALLAH A.I. ALI, MOHAMMED PATEL, ANDREW D. ELLIS

Aston Institute of Photonic Technologies, Aston University, Birmingham, B4 7ET, United Kingdom.
**Corresponding author: y.li70@aston.ac.uk*

Received XX Month XXXX; revised XX Month, XXXX; accepted XX Month XXXX; posted XX Month XXXX (Doc. ID XXXXX); published XX Month XXXX

We employ commercial mode-selective photonic lanterns to implement mode multiplexing and demultiplexing for high-capacity free-space optical communications. Moreover, we design a time-division-multiplexed frame structure to efficiently emulate multiple independent transmitters with channelized precoding using only one transmitter. To maximize the throughput of the system, we optimize the modes selected for carrying data, and apply adaptive loading to different channels. By leveraging mode- and polarization-division multiplexing, the free-space optical data link comprising multiple independent channels provides an aggregate net data rate of 1.1 Tbit/s and net spectral efficiency of 28.35 bit/s/Hz. Different from many previous demonstrations based on delayed or partially delayed copies of identical data streams, to the best of our knowledge, it is a record-high net data rate and net spectral efficiency achieved by a single-wavelength mode-division multiplexed free-space optical communication system with fully independent channels. Moreover, all key devices used in this work, including optical transponder, multiplexer and demultiplexer are commercially available.

http://dx.doi.org/10.1364/OL.99.099999

Mode-division multiplexed (MDM) transmission over a free-space optical (FSO) link has been widely investigated due to its potential to deploy additional capacity without the expense of installing additional fiber links. Orbital angular momentum (OAM) is one of the most popular modal basis sets chosen by many researchers [1], [2]. However, due to the sacrifice of its radial degrees of freedom, OAM is only a subset of the Laguerre-Gaussian (LG) modal basis set in free space. Therefore, for a given aperture size, compared to other complete orthogonal basis sets, such as LG modes, Hermite–Gaussian (HG) modes and linearly polarized (LP) modes, OAM-based MDM optical communication systems provide lower bandwidth capacity [3]. To cope with this challenge, some studies leveraging the complete modal basis have been reported [4], [5].

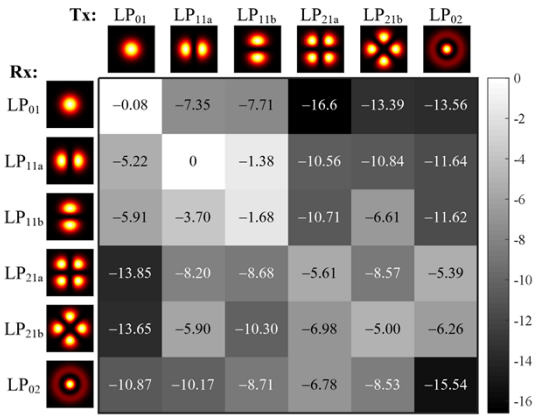

Fig. 1. Measured crosstalk matrix (dB) of MSPL, normalized to LP_{11a}.

Alternative spatial mode multiplexing techniques include shaping the wavefront of the light by using q-plates [6], phase plates [7] or spatial light modulators [8], and achieving in-fiber mode conversion by using 3D waveguides [9-11], e.g., mode-selective photonic lanterns (MSPLs) [10], [11]. There have been many reported demonstrations using MDM to increase the system capacity over an FSO link [4], [12-14]. However, most of them shape the wavefront of the light using non-commercial devices in free space for multiplexing and demultiplexing. Only few MDM-FSO demonstrations have been realized by in-fiber mode conversion, which potentially has lower power loss as well as higher operational stability and device flexibility [15] in hybrid fiber/FSO communication systems.

In this Letter, we employ a MDM transmitter system comprising a commercial transponder and commercial MSPLs, along with a convenient burst mode channel emulation technique, to excite LP modes for MDM transmission. These fiber-based mode

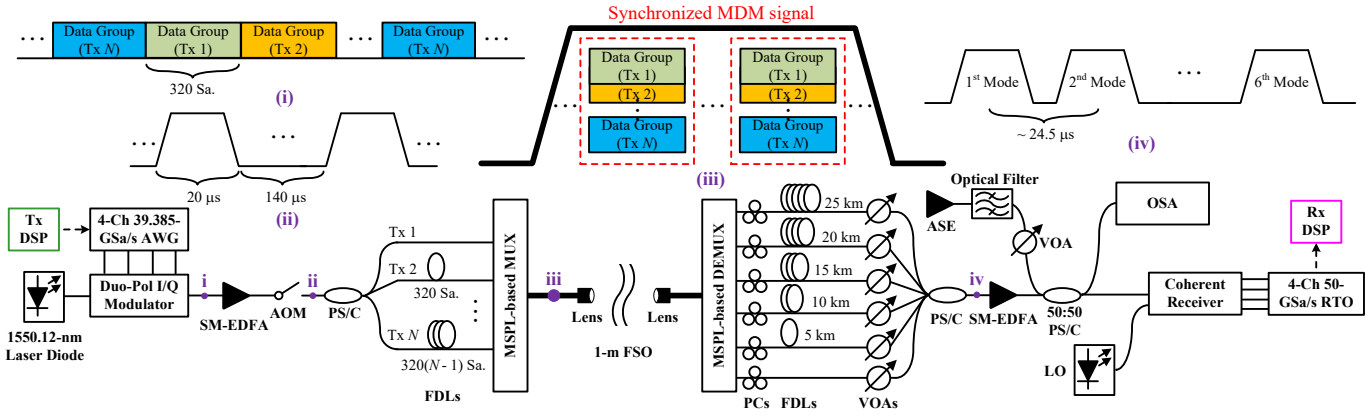

Fig. 2. Proof-of-concept experiment for demonstrating a MIMO MDM-FSO communication system using the TDM frame structure and TDM receiver (ASE: amplified spontaneous emission; LO: local oscillator; OSA: optical spectrum analyzer; RTO: real-time oscilloscope). Insets: (i) Frame structure of the transmitted TDM-SM signal; (ii) Signal bursts after AOM; (iii) Synchronized MDM signal bursts after passing through FDLs and multiplexing; (iv) Received TDM-SM signal bursts after demultiplexing and interleaving.

multiplexers/demultiplexers are capable of achieving low mode-dependent loss (MDL), low insertion loss, and low coupling loss in theory [10], [11]. It should be noted that the LP modes excited by a MSPL can be approximated by a scale-adapted set of LG modes in free space [16]. Meanwhile, we utilize a time-division-multiplexed (TDM) frame structure and fiber delay decorrelation to emulate a multi-input multi-output (MIMO) MDM-FSO communication system comprising fully independent channels and enabling channelized precoding, which is different from many of the previous studies [12], [13] that are based on delayed or partially delayed copies of identical data streams. By optimizing the MDM-FSO system and leveraging adaptive loading, we successfully demonstrate a net data rate of 1.1 Tbit/s across the 5 lowest order LP modes, and a net spectral efficiency of 28.35 bit/s/Hz. To the best of our knowledge, it is a record-high net data rate and net spectral efficiency achieved by a single-wavelength MDM-FSO communication system using commercial devices.

As shown in Fig. 1, we first measured the normalized crosstalk matrix of the pair of commercial 6-mode MSPLs (Phoenix Photonics Ltd) used in this work. We can see from the figure that whilst there is a strong diagonal component for the three lowest order modes, the commercial MSPL-based multiplexer and demultiplexer induced relatively strong inter-mode crosstalk, especially for the highest-order mode (LP_{02}). Therefore, we only used the first N modes, where $N \leq 5$, at the transmitter side for MDM transmission, and used all 6 modes at the receiver side for robust reception [17]. It should be noted from the figure that the overall received power of each transmit mode (column) is different, which can be attributed to the residual MDL of the MSPLs. Meanwhile, in potential applications, the effects of crosstalk and MDL could be further increased by turbulence [2]. Since different crosstalk and MDL result in different signal-to-noise ratios (SNRs) of different channels, bit and power allocation based on Chow's adaptive loading algorithm [18] is applied to all channels to maximize the throughput of our system. Multiple independent transmitters and receivers are thus required. To emulate them in a MIMO MDM system with only one coherent transmitter and one coherent receiver, we have designed a TDM frame structure in digital signal processing (DSP) with the existing TDM receiver [19] as shown in Fig. 2.

At the transmitter side, after DSP, a dual-polarization (DP) quadrature amplitude modulation (QAM) optical signal at 1550.12 nm was generated in a commercial line card where the DP-I/Q modulator was driven by the onboard 4-channel 39.385-GSa/s arbitrary waveform generator (AWG). We can see from Fig. 2(i) that the signal was divided into consecutive TDM data groups, where each data group carried the data allocated to a certain transmitter to be emulated and had a length of 320 samples (~8.1 ns). To compensate for the relatively large insertion loss (~10.2 dB) induced by the 1×8 power splitter/coupler (PS/C) employed at the transmitter side, a single-mode (SM) erbium-doped fiber amplifier (EDFA) first amplified the signal to 20 dBm, after which the signal was sent into an acousto-optic modulator (AOM) set to switch at a period of 160 µs with a duty cycle of 12.5% to generate 20-µs signal bursts (~2,462 data groups) as shown in Fig. 2(ii). The PS/C was then employed to split the signal bursts into N channels, emulating N independent transmitters. All the channels were decorrelated by an array of variable fiber delay lines (FDLs) before mode-division multiplexing via a commercial 6-mode MSPL. As shown in the figure, each delay line had a length of 320(n - 1) samples, where n was the index of transmitters. Each path was aligned to within 2% of a sample period. Besides implementing decorrelation of channels, as shown in Fig. 2(iii), the data groups representing different transmitters can also be synchronized after passing through FDLs and multiplexing. Although the unsynchronized data groups will be discarded from the final performance evaluation, the synchronized data groups taking up $1/N$ of the total data can efficiently emulate a MDM signal with N independent transmitters in practical applications. The MDM signal within a few-mode fiber was then coupled into free space using an achromatic lens (50-mm diameter, 100-mm focal length) for ~1-m FSO transmission.

At the receiver side, another achromatic lens was employed to couple the beam into a few-mode fiber, where the overall coupling loss was ~5.3 dB. The MDM signal was then sent into another commercial 6-mode MSPL for demultiplexing, after which the power difference between two polarization states (X and Y) of the SM signals was minimized by 6 polarization controllers (PCs). 6 independent receivers for the reception of 6 modes can then be emulated by another array of FDLs and PS/C, where the FDLs had a difference in length of ~5 km, delaying the signals by ~24.5 µs as shown in Fig. 2(iv). Before interleaving, an array of variable optical attenuators (VOAs) was employed to balance the received power in

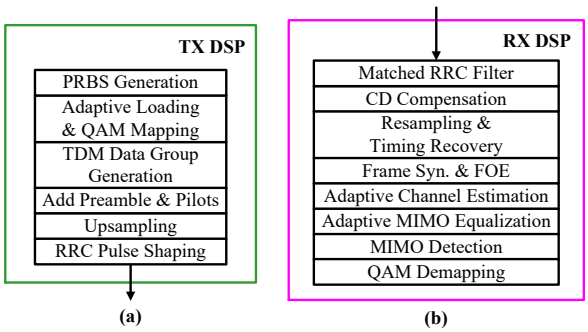

Fig. 3. Block diagrams of the offline DSP at (a) the transmitter side and (b) the receiver side.

different modes. The TDM signal bursts were then amplified to 7 dBm by another SM-EDFA to minimize the quantization noise before being noise-loaded. The optical signal-to-noise ratio (OSNR) was varied by another VOA, and the average OSNR was measured by an optical spectrum analyzer. After coherent detection by a coherent receiver with a free-running local oscillator, 4 resultant electrical signals were finally acquired by a 4-channel real-time oscilloscope working at 50 GSa/s for the offline DSP.

Fig. 3(a) and Fig. 3(b) show the DSP used at the transmitter side and the receiver side, respectively. At the transmitter side, the generated pseudorandom binary sequence (PRBS) was first mapped onto QAM symbols with both bit and power loading based on the prior knowledge of channel state information [18], which can be estimated by training sequences before transmission. The optimized QAM symbols were then used to construct a TDM payload signal as shown in Fig. 2(i). Each frame of the signal consisted of 49 × N data groups, in which a preamble for frame synchronization and frequency offset estimation (FOE) was inserted as the start of a frame, as shown in Fig. 4, where N = 3 for illustration. The proposed structure of the preamble consists of two symmetric sequences. It can be written as $\boldsymbol{P}_n = [\mathbf{A}_n; \mathbf{B}_n]$ for the n^{th} transmitter, where $\boldsymbol{B}_n$ is symmetric with respect to $\boldsymbol{A}_n$. Particularly in this work, $\boldsymbol{P}_n$ had a length of 320 samples after AWG, and had the same TDM structure as the payload, as illustrated in Fig. 4(a), leading to an overhead of 2% (= 1 / (49 + 1)). Pilots (10% overhead) were then added to all groups for the adaptive channel estimation and equalization at the receiver side. Before being sent to the AWG, the signal was up-sampled to 39.385 GSa/s and root-raised cosine (RRC) pulse shaped (0.05 roll-off factor) to achieve better transmission performance.

At the receiver side, matched RRC filtering, chromatic dispersion (CD) compensation, resampling and timing recovery were applied to the received signal before performing the frame synchronization and the FOE by utilizing the proposed preamble. If we assume that the MIMO channel is quasi-static, the two half sequences of the received preamble still maintain the symmetry property even with strong inter-channel crosstalk, as illustrated in Fig. 4(b). We can then blindly find the maximum timing metric [20] by sliding a window of the same size as $\boldsymbol{P}_n$. However, in practical applications, the whole MIMO channel is time-varying, especially for its phase component which is mainly affected by phase noise and frequency offset. Therefore, in the proposed scheme, we only use their intensity information to calculate the timing metric for robust frame synchronization. Compared to the conventional repetitive preamble structure, the symmetric structure shows higher robustness [21]. Meanwhile, different from some existing schemes

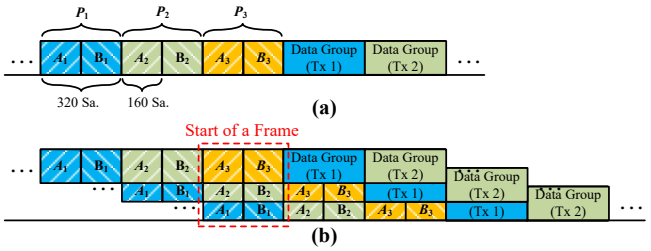

Fig. 4. Illustration of preambles (a) inserted at the transmitter side, and (b) after splitter, FDLs and multiplexing, where N = 3.

[21], the proposed preamble can also be used for blind FOE in the frequency domain, as

$$\Delta f_m = \frac{1}{2TL}\arg\max_{k,|k|\le L/2}\left|\sum_{l=0}^{L-1} r_m^*(L-l-1)\,r_m(L+l)\,e^{-j\frac{2\pi lk}{L}}\right|, \quad \textbf{(1)}$$

where Δf_m is the estimated frequency offset at the m^{th} receiver; T denotes the symbol period; r_m is the synchronized preamble at the m^{th} receiver, which has a length of $2L$; $(\cdot)^*$ denotes the complex conjugate operation. After compensation for Δf_m, the transfer matrices containing both amplitude and phase information of the MIMO channel were adaptively estimated via pilots, which were then used for both inter-symbol interference mitigation and inter-mode crosstalk elimination. In this work, different from the traditional MIMO equalization, these two parts were respectively realized by adaptive MIMO equalization and MIMO detection to achieve improved flexibility. Although we only used a simple minimum mean square error (MMSE) decoder in this work, it can be easily replaced by other advanced MIMO detection algorithms, e.g., successive interference cancellation [17] and maximum likelihood decoding, for better performance at the expense of complexity. The transmission performance was finally evaluated by calculating the bit error rate (BER) after QAM demapping.

Fig. 5 presents the experimental results. In Fig. 5(a) and Fig. 5(b), we first compare the transmission performance of the MDM signals with and without adaptive loading. For a fair comparison, the data rate of all signals is fixed at 885 Gbit/s by allocating 30 bits to all 10 channels (2 polarizations × 5 modes) and setting the symbol rate to 29.5 Gbaud. To verify the feasibility of the robust reception using all 6 receivers, we also evaluated the performance of the MDM-FSO system with only the first 5 receivers. We can see from Fig. 5(a) that the adaptive loading can bring on performance improvement for both cases, i.e., ~4-dB OSNR sensitivity improvement when using only 5 receivers and ~3.5-dB OSNR sensitivity improvement when using all 6 receivers, at the hard-decision forward error correction (HD-FEC) threshold of 4.7×10^{-3} [22]. Moreover, we can see from Fig. 5(a) that one more receiver can provide more power as well as more information for detection, leading to ~4-dB OSNR sensitivity improvement. The performance improvement from adaptive loading can be explained by Fig. 5(b), where the average OSNR of two signals is fixed at 27.04 dB. In the case without adaptive loading, the BER of different channels shows a very large fluctuation due to the difference in SNR in our MIMO system. Meanwhile, this problem can be effectively solved by allocating different modulation formats and power to different channels based on the SNR estimated before transmission [18]. The average BER is thus reduced from 6.28×10^{-3} to 1.56×10^{-3}, meeting the requirement of HD-FEC.

We finally maximized the throughput of our MDM-FSO system by leveraging adaptive loading as shown in Fig. 5(c). Herein, we varied

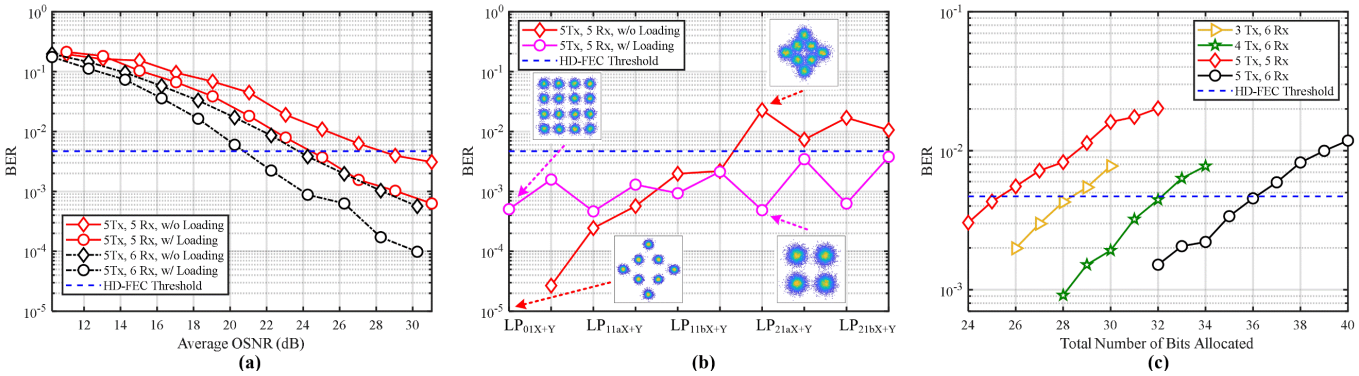

Fig. 5. (a) Transmission performance of different signals at the same data rate (30 bits, 29.5 Gbaud). (b) BER versus channel index for the signals with and without adaptive loading (30 bits, 29.5 Gbaud, average OSNR = 27.04 dB). (c) Throughput maximization with adaptive loading and different schemes (36.9 Gbaud).

the number of transmitters and the total number of bits allocated. The number of receivers was fixed at 6, except the case with 5 transmitters and 5 receivers was attached as the benchmark. The symbol rate was set to 36.9 Gbaud for all cases. We can see from the figure that by enabling the first 5 modes for carrying data, we successfully achieved a maximum line rate of ~1.33 Tbit/s (≈ 36 bits × 36.9 Gbaud). After considering the 0.05 roll-off factor and the overhead of preamble (2%), pilots (10%) and HD-FEC (6.25%), the net data rate and the net spectral efficiency achieved in this work are ~1.1 Tbit/s and 28.35 bit/s/Hz, respectively.

In this Letter, we have demonstrated a TDM frame structure to efficiently emulate multiple independent transmitters in a MDM system. We have also demonstrated the use of a symmetric preamble structure for simultaneously realizing blind frame synchronization and FOE. With this scheme and the conventional TDM receiver, we applied adaptive loading to a MDM-FSO system suffering from relatively strong crosstalk, and have successfully achieved, to the best of our knowledge, a record high net single-wavelength data rate of 1.1 Tbit/s and spectral efficiency of 28.35 bit/s/Hz using commercial transponder and MSPLs. These results verify the effectiveness of the scheme and the potential of leveraging the complete modal basis in MDM-FSO systems for ultra-high-speed transmission.

Funding. This work was supported by the UK EPSRC (Grants EP/T009047/1, EP/S003436/1, and EP/S016171/1) and H2020 Marie Skłodowska- Curie Actions (713694).

Acknowledgments. The authors would like to thank Ciena and Dr. Charles Laperle for kindly providing the WaveLogic 3 transponder used in our experiments.

Disclosures. The authors declare no conflicts of interest.

Data availability. The data that support the figures within this Letter are available from Aston Data Explorer (DOI: 10.17036/researchdata.aston.ac.uk.00000540).

References

1. A. Trichili, C. Rosales-Guzmán, A. Dudley, B. Ndagano, A. B. Salem, M. Zghal, and A. Forbes, Sci. Rep. **6**, 27674 (2016).
2. A. E. Willner, Z. Zhao, C. Liu, R. Z. Zhang, H. Q. Song, K. Pang, K. Manukyan, H. Song, X. Z. Su, G. D. Xie, Y. X. Ren, Y. Yan, M. Tur, A. F. Molisch, R. W. Boyd, H. B. Zhou, N. Z. Hu, A. Minoofar, and H. Huang, APL Photonics **6**(3), 030901 (2021).
3. N. Zhao, X. Li, G. Li, and J. M. Kahn, Nat. Photonics **9**(12), 822–826 (2015).
4. K. Pang, H. Song, Z. Zhao, R. Zhang, H. Song, G. Xie, L. Li, C. Liu, J. Du, and A. F. Molisch, Opt. Lett. **43**(16), 3889–3892 (2018).
5. M. A. Cox, L. Maqondo, R. Kara, G. Milione, L. Cheng, and A. Forbes, J. Lightwave Technol. **37**(16), 3911–3917 (2019).
6. G. Milione, M. P. J. Lavery, H. Huang, Y. Ren, G. Xie, T. A. Nguyen, E. Karimi, L. Marrucci, D. A. Nolan, R. R. Alfano, and A. E. Willner, Opt. Lett. **40**(9), 1980–1983 (2015).
7. P. Genevaux, C. Simonneau, G. Labroille, B. Denolle, O. Pinel, P. Jian, J. F. Morizur, and G. Charlet, in Optical Fiber Conference 2015, paper W1A.5.
8. N. K. Fontaine, R. Ryf, H. Chen, D. T. Neilson, K. Kim, and J. Carpenter, Nat. Commun. **10**, 1865 (2019).
9. J. Dong, K. S. Chiang, and W. Jin, J. Lightwave Technol. **33**(22), 4580–4588 (2015).
10. S. G. Leon-Saval, N. K. Fontaine, J. R. Salazar-Gil, B. Ercan, R. Ryf, and J. Bland-Hawthorn, Opt. Express **22**(1), 1036–1044 (2014).
11. T. A. Birks, I. Gris-Sánchez, S. Yerolatsitis, S. Leon-Saval, and R. R. Thomson, Adv. Opt. Photon. **7**(2), 107–167 (2015).
12. H. Huang, G. Xie, Y. Yan, N. Ahmed, Y. Ren, Y. Yue, D. Rogawski, M. Tur, B. Erkmen, K. Birnbaum, S. Dolinar, M. Lavery, M. Padgett, and A. E. Willner, Optical Fiber Conference 2013, paper OTh4G.5.
13. J. Wang, S. Li, M. Luo, J. Liu, L. Zhu, C. Li, D. Xie, Q. Yang, S. Yu, J. Sun, X. Zhang, W. Shieh, and A. E. Willner, in European Conference on Optical Communication, Cannes, France, (2014), paper Mo.4.5.1.
14. J. Zhang, F. Li, J. Li, Y. Feng, and Z. Li, IEEE Photonics J. **8**(6), 7907008 (2016).
15. Z. S. Eznaveh, J. C. A. Zacarias, J. E. A. Lopez, K. Shi, G. Milione, Y. Jung, B. C. Thomsen, D. J. Richardson, N. Fontaine, S. G. J. O. e. Leon-Saval, and R. A. Correa, Opt. Express **26**(23), 30042–30051 (2018).
16. R. Brüning, Y. Zhang, M. McLaren, M. Duparré, and A. Forbes, J. Opt. Soc. Am. A **32**(9), 1678–1682 (2015).
17. Y. Li, Z. Hu, D.M. Benton, A. Ali, M. Patel, and A.D. Ellis, Opt. Lett. **47**(11), 2742-2745 (2022).
18. P. S. Chow, J. M. Cioffi, and J. A. Bingham, IEEE Trans. Commun., **43**(2/3/4), 773–775 (1995).
19. R. G. H. van Uden, C. M. Okonkwo, H. Chen, H. de Waardt, and A. M. J. Koonen, Opt. Express **22**(10), 12668–12677 (2014).
20. T.M. Schmidl and D. C. Cox, IEEE Trans. Commun., **45**(12), 1613–1621 (1997).
21. J. Lu, Q. Wu, H. Jiang, S. Fu, M. Tang, and C. Lu, J. Lightw. Technol., **37**(20), 5299-5308 (2019).
22. L. M. Zhang and F. R. Kschischang, J. Light. Technol., **32**(10), 1999 (2014).

References (Full)

1. A. Trichili, C. Rosales-Guzmán, A. Dudley, B. Ndagano, A. B. Salem, M. Zghal, and A. Forbes, "Optical communication beyond orbital angular momentum," Sci. Rep. **6**, 27674 (2016).
2. A. E. Willner, Z. Zhao, C. Liu, R. Z. Zhang, H. Q. Song, K. Pang, K. Manukyan, H. Song, X. Z. Su, G. D. Xie, Y. X. Ren, Y. Yan, M. Tur, A. F. Molisch, R. W. Boyd, H. B. Zhou, N. Z. Hu, A. Minoofar, and H. Huang, "Perspectives on advances in high-capacity, free-space communications using multiplexing of orbital-angular-momentum beams," APL Photonics **6**(3), 030901 (2021).
3. N. Zhao, X. Li, G. Li, and J. M. Kahn, "Capacity limits of spatially multiplexed free-space communication," Nat. Photonics **9**(12), 822–826 (2015).
4. K. Pang, H. Song, Z. Zhao, R. Zhang, H. Song, G. Xie, L. Li, C. Liu, J. Du, and A. F. Molisch, "400-gbit/s qpsk free-space optical communication link based on four-fold multiplexing of hermite–gaussian or laguerre–gaussian modes by varying both modal indices," Opt. Lett. **43**(16), 3889–3892 (2018).
5. M. A. Cox, L. Maqondo, R. Kara, G. Milione, L. Cheng, and A. Forbes, "The resilience of hermite-and laguerregaussian modes in turbulence," J. Lightwave Technol. **37**(16), 3911–3917 (2019).
6. G. Milione, M. P. J. Lavery, H. Huang, Y. Ren, G. Xie, T. A. Nguyen, E. Karimi, L. Marrucci, D. A. Nolan, R. R. Alfano, and A. E. Willner, "4 × 20 Gbit/s mode division multiplexing over free space using vector modes and a q-plate mode (de) multiplexer," Opt. Lett. **40**(9), 1980–1983 (2015).
7. P. Genevaux, C. Simonneau, G. Labroille, B. Denolle, O. Pinel, P. Jian, J. F. Morizur, and G. Charlet, "6-mode Spatial Multiplexer with Low Loss and High Selectivity for Transmission over Few Mode Fiber," in Optical Fiber Conference 2015, paper W1A.5.
8. N. K. Fontaine, R. Ryf, H. Chen, D. T. Neilson, K. Kim, and J. Carpenter, "Laguerre-Gaussian mode sorter," Nat. Commun. **10**, 1865 (2019).
9. J. Dong, K. S. Chiang, and W. Jin, "Compact three-dimensional polymer waveguide mode multiplexer," J. Lightwave Technol. **33**(22), 4580–4588 (2015).
10. S. G. Leon-Saval, N. K. Fontaine, J. R. Salazar-Gil, B. Ercan, R. Ryf, and J. Bland-Hawthorn, "Mode-selective photonic lanterns for space-division multiplexing," Opt. Express **22**(1), 1036–1044 (2014).
11. T. A. Birks, I. Gris-Sánchez, S. Yerolatsitis, S. Leon-Saval, and R. R. Thomson, "The photonic lantern," Adv. Opt. Photon. **7**(2), 107–167 (2015).
12. H. Huang, G. Xie, Y. Yan, N. Ahmed, Y. Ren, Y. Yue, D. Rogawski, M. Tur, B. Erkmen, K. Birnbaum, S. Dolinar, M. Lavery, M. Padgett, and A. E. Willner, "100 Tbit/s Free-Space Data Link using Orbital Angular Momentum Mode Division Multiplexing Combined with Wavelength Division Multiplexing," in Optical Fiber Conference 2013, paper OTh4G.5.
13. J. Wang, S. Li, M. Luo, J. Liu, L. Zhu, C. Li, D. Xie, Q. Yang, S. Yu, J. Sun, X. Zhang, W. Shieh, and A. E. Willner, "N-dimensional multiplexing link with 1.036-Pbit/s transmission capacity and 112.6-bit/s/Hz spectral efficiency using OFDM-8QAM signals over 368 WDM pol-muxed 26 OAM modes," in European Conference on Optical Communication, Cannes, France, (2014), paper Mo.4.5.1.
14. J. Zhang, F. Li, J. Li, Y. Feng, and Z. Li, "120 Gbit/s 2× 2 vector-modes-division-multiplexing DD-OFDM32QAM free-space transmission," IEEE Photonics J. **8**(6), 7907008 (2016).
15. Z. S. Eznaveh, J. C. A. Zacarias, J. E. A. Lopez, K. Shi, G. Milione, Y. Jung, B. C. Thomsen, D. J. Richardson, N. Fontaine, S. G. J. O. e. Leon-Saval, and R. A. Correa, "Photonic lantern broadband orbital angular momentum mode multiplexer," Opt. Express **26**(23), 30042–30051 (2018).
16. R. Brüning, Y. Zhang, M. McLaren, M. Duparré, and A. Forbes, "Overlap relation between free-space Laguerre Gaussian modes and step-index fiber modes," J. Opt. Soc. Am. A **32**(9), 1678–1682 (2015).
17. Y. Li, Z. Hu, D.M. Benton, A. Ali, M. Patel, and A.D. Ellis, "Demonstration of 10 channel mode- and polarization-division multiplexed free-space optical transmission with successive interference cancellation DSP," Opt. Lett. **47**(11), 2742-2745 (2022).
18. P. S. Chow, J. M. Cioffi, and J. A. Bingham, "A practical discrete multitone transceiver loading algorithm for data transmission over spectrally shaped channels," IEEE Trans. Commun., **43**(2/3/4), 773–775 (1995).
19. R. G. H. van Uden, C. M. Okonkwo, H. Chen, H. de Waardt, and A. M. J. Koonen, "Time domain multiplexed spatial division multiplexing receiver," Opt. Express **22**(10), 12668–12677 (2014).
20. T.M. Schmidl and D. C. Cox, "Robust frequency and timing synchronizationfor OFDM," IEEE Trans. Commun. **45**(12), 1613–1621 (1997).
21. J. Lu, Q. Wu, H. Jiang, S. Fu, M. Tang, and C. Lu, "Efficient Timing/Frequency Synchronization Based on Sparse Fast Fourier Transform (S-FFT)," J. Lightw. Technol., **37**(20), 5299-5308 (2019).
22. L. M. Zhang and F. R. Kschischang, "Staircase codes with 6% to 33% overhead," J. Light. Technol., **32**(10), 1999–2002 (2014).